AN INTEGRATED APPROACH TO COMPUTE PHYSICAL PROPERTIES OF CORE SAMPLES

S. Linden[(1,2)], T. Cvjetkovic[(2)], E. Glatt[(2)] and A. Wiegmann[(2)]
[(1)]Fraunhofer ITWM, Fraunhofer-Platz 1, 67665 Kaiserslautern, Germany
[(2)]Math2Market GmbH, Trippstadter Str. 110, 67663 Kaiserslautern, Germany

This paper was prepared for presentation at the International Symposium of the Society of Core Analysts held in Avignon, France, 8-11 September, 2014.

ABSTRACT

We introduce an integrated approach to compute physical properties of core samples on very large micro-CT images and nano-CT images. On the same segmented 3d image, a whole range of diverse effective material properties are computed. In addition, we study the behavior of these material properties under compression. Where data is available, our methods are compared to other state of the art solvers on a large complex Berea sandstone dataset [1]. Our newest flow solver is 3-6 times faster than the fastest solver in [2], scales well for up to 32 processors and promises to solve 3k by 3k by 3k domains in as little as 180GB of memory. An additional benefit of this work is that the reported range of permeabilities from the benchmark [2] can be narrowed down significantly.

INTRODUCTION

Geoscientists are interested in effective material properties of core samples. On segmented 3d images, we find

1. the Permeability in 3 directions and the permeability tensor
2. the Tortuosity, based on computing the effective gas diffusivity
3. the Electrical conductivity (& formation factor), assuming that the solid phase is non conductive
4. the Drainage curve, simulating air intrusion in an initially wet medium
5. the Resistivity index for partial brine saturation
6. the Stiffness tensor
7. the deformation of the sample under uniform external pressure
8. the properties 1.-3. on the compressed sample

These microscopic properties can be used in macroscopic simulations to predict and enhance oil production processes. The increase of pressure below ground level can lead to different results when experimenting with core samples at the surface. Therefore, it is interesting to study the effective properties under simulated high pressure conditions.

METHODS

Five numerical methods are used to predict effective physical properties. We depict basic ideas but refer to corresponding literature for a more detailed description. All methods are designed to deal with large and complex segmented 3D images (voxel geometries).

Simple-FFT for the Stokes Equations

The Semi implicit methods for pressure linked equations (SIMPLE) are used to solve the (Navier-)Stokes equations. The stationary Stokes equations are defined by

$$\begin{aligned} \mu\Delta u - \nabla p &= 0 \\ \nabla \cdot u &= 0 \end{aligned} \qquad (1)$$

where u, p, μ are velocity, pressure and viscosity, respectively. The method is decomposed into the following steps: guess a pressure field, solve the momentum conservation equation, correct the pressure field with respect to mass conservation and correct the velocity field. We use the recent enhancement of the original algorithm called SIMPLE-FFT [3]. The linear equation for the pressure correction is solved by using fast Fourier transforms. The number of iterations required for low porous geometries is reduced significantly.

Explicit Jump for Electrical Conduction and Diffusion Equation

Explicit-Jump immersed interface method is a very fast finite difference method to solve partial differential equations [4,5]. It can be used to solve the electrical conduction and diffusion equation

$$\nabla \cdot (\beta \nabla U) = f \qquad (2)$$

where U denotes the potential and $\beta > 0$ the piecewise constant conductivity. Additional jump variables across material interfaces are introduced to represent discontinuities inside the flux. Conductivities at the jumps are determined by harmonic averaging. The problem can be reformulated such that the solution variables for the potentials are neglected and jump variables are kept. The fast convergence rate is achieved by using the fast Fourier transforms and depends on the number of jumps.

Pore Morphology for Two-Phase Drainage Simulation

The pore morphology method allows determining the distribution of a wetting and a non-wetting phase inside a porous medium [6, 7, 8]. Capillary pressure curves and relative quantities with respect to saturation can be predicted. The methods consists of three steps: Assigning a pore size to each voxel, drainage or imbibition based on connected pore size paths and determination of the capillary pressure p_c using the Young-Laplace equation

$$p_c = \frac{2\gamma}{r} \qquad (3)$$

with surface tension γ and sphere radius r. Relative permeabilities and conductivities can then be computed by flow or diffusion solvers, respectively.

Lippmann Schwinger for Linear Elasticity

The implementation described in [9] is used to compute effective elastic moduli, i.e. the stiffness tensor and to predict large deformations of a given medium. For a uniform macroscopic strain we solve a boundary value problem (BVP) for the displacement field. The BVP consists of the elastic equilibrium equation, Hooke's law and periodic boundary conditions. By introducing a reference material of homogeneous stiffness C_0 the BVP can be transformed into the strain ϵ based Lipmann-Schwinger equation

$$\varepsilon = \Gamma_0 * \left((C - C_0) : \epsilon\right) = E \quad (4)$$

Fast Fourier transforms allows to solve the convolution of the Green operator Γ_0. The number of iterations depends on the phase contrast.

LIR-Tree with Conservative Cellular Structure for the Stokes Equations

The LIR-tree is a generalization of the Octree and KD-tree based on the ternary alphabet A={L,I,R} and is designed to represent huge voxel geometries in a numerically suitable way. The images are coarsened in areas where the velocity and pressure do not vary much while keeping the original high resolution near the solid surfaces. Variables are arranged so that each cell is able to satisfy the Stokes-equation independently from its neighbor cells [10]. Pressure and velocity are discretized on staggered grids but instead of using one velocity variable on the cell faces we introduce two velocity variables.

RESULTS

In our experiments we use a segmentation of a computed tomography scan from Berea sandstone described in [1]. The dataset is included in the benchmark study [2] where only permeability, electric conductivity and elastic moduli are considered. We extend this list of properties by the tortuosity factor, diffusivity, capillary pressure curve and the resistivity index. In addition, we study the behavior of the mentioned properties under compression. Figure 1 shows the voxel geometry of the Berea sandstone dataset with 720×720×1024 voxels and a resolution of 0.74 μm per voxel. A visualization of the velocity field and the von Mises stress is shown in Figure 2 and Figure 3, respectively.

Permeability, tortuosity factor, diffusivity, conductivity and formation factor in z-direction for three compression levels are shown in Table **1**. The values fall within the expected range for the none-compressed case.

Figure 5 indicates a quadratic decrease of permeability with respect to compression. This corresponds to diameter dependent laminar flow profiles in a tube. The permeabilites are computed with the SIMPLE-FFT and the LIR-solver with almost the same results. The values are in the middle of the reported ones [101, 119] mD in the benchmark study [2].

The tortuosity factor, diffusivity, conductivity and the formation factor have a linear fall-off with respect to compression. This corresponds to the linear relation of flux and diameter. Figure 6 shows the linear behavior of the formation factor.

Compression	Permeability	Tortuosity Factor	Diffusivity	Conductivity	Formation Factor
	[mD]	[-]	[%]	[S/m]	[-]
0%	107	4.65	3.96	0.198	25.2
1%	61.9	5.65	2.77	0.139	36.1
2%	30	7.6	1.72	0.086	58
3%	18.8	9.16	1.3	0.065	77

Table 1 Permeability, tortuosity, diffusivity, conductivity and formation factor for different compressions. The Berea dataset is compressed along the z-direction. Effective properties are also computed for that direction as well.

Figure 1 Berea sandstone.

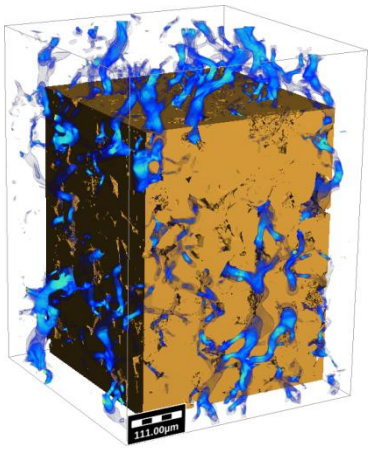

Figure 2 Velocity field.

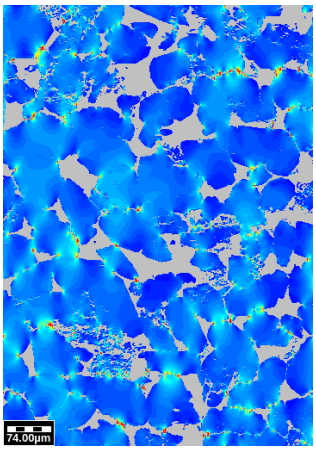

Figure 3 Von Mises stress.

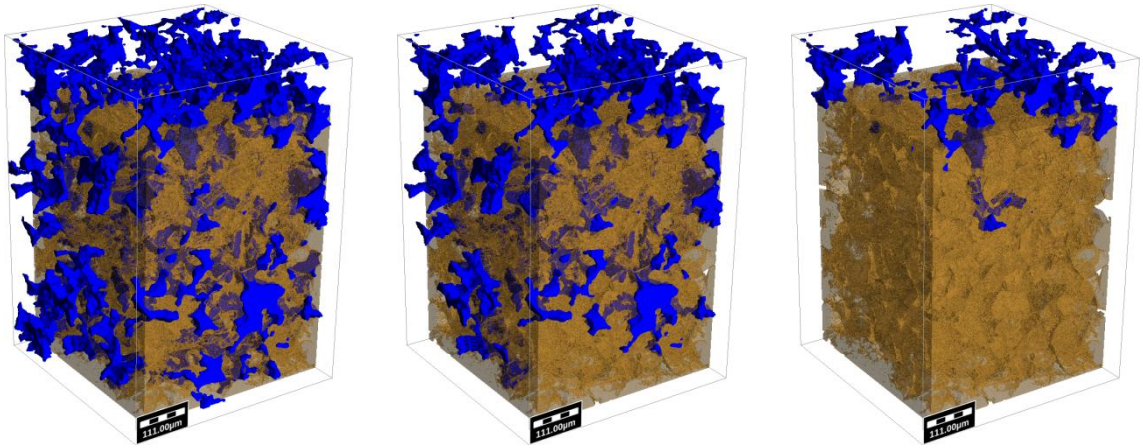

Figure 4 Brine saturation with 60%, 40% and 20%. Air intrudes from bottom to top.

The computed elastic modulus is $E = 45.9$ and the poisson ratio is $\upsilon = 0.108$ for the uncompressed geometry. The stiffness tensor indicates an isotropic medium and the elastic properties match with reported values in literature for Berea sandstone. The simulation does consider multiple solid materials since the segmentation consists of only two phases: pore and sandstone.

The drainage curve for air intrusion in an initially wet medium and the resistivity index for partial brine saturation are computed by the pore morphology and the explicit jump method. Figure 4 shows the intrusion of air from the top of the domain for three stages while Figure 7 and Figure 8 show the corresponding graphical course.

The runtimes and memory requirements are shown in Table **2** where we used a computer with 16 cores and 128 GB of RAM. The computation of Stokes flows and linear elastic problems requires the most runtime. For the Stokes equations the LIR solver requires less runtime and memory compared to the SIMPLE-FFT due to the adaptive discretization. EJ-diff and EJ-cond have almost the same runtime and memory requirement since they solve the same numerical problem.

Method	S-FFT	LIR	EJ-diff	EJ-cond	LS
Runtime [h]	26.4	14	10.9	11	22.6
Memory [GB]	40.5	5.8	10.6	10.6	97.1

Table 2 Runtime and memory requirements of the PDE solvers. The runtimes include three load cases for S-FFT, LIR, EJ and six load cases for the LS solver.

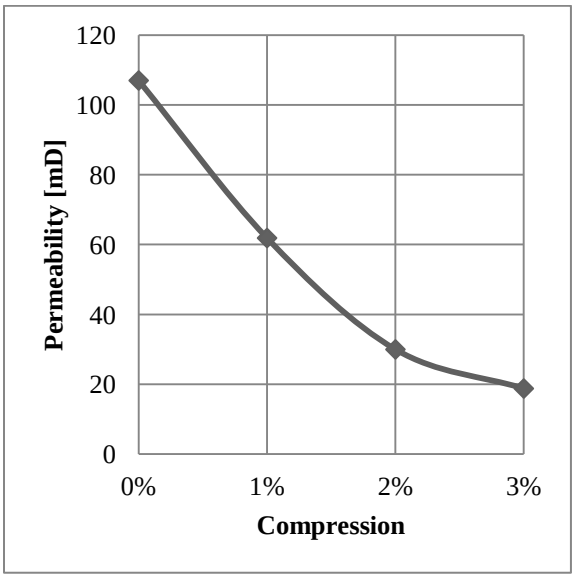

Figure 5 Permeability for different compressions.

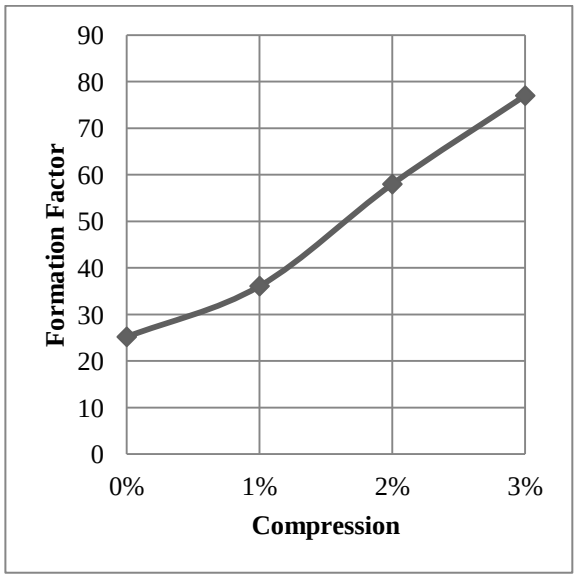

Figure 6 Formation factor for different compressions.

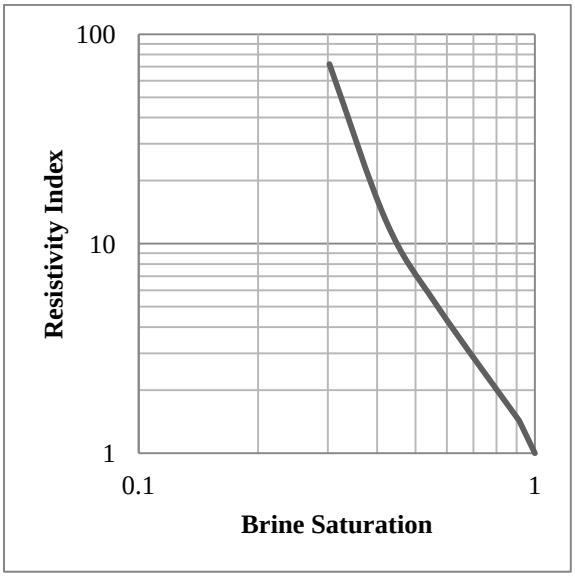

Figure 7 Resistivity index for different brine saturations.

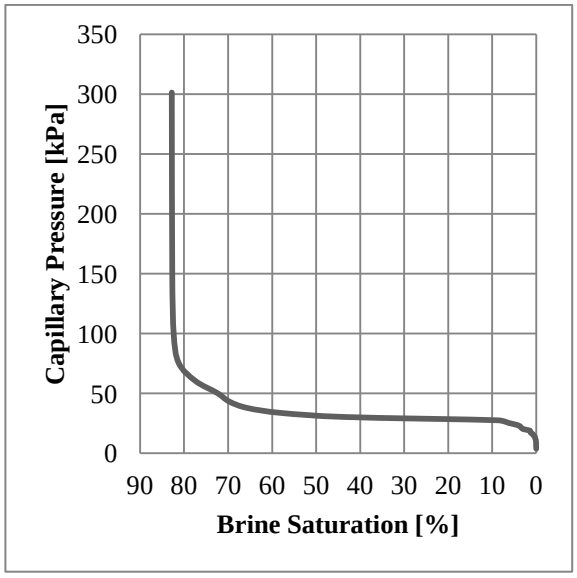

Figure 8 Capillary pressure for different brine saturations.

CONCLUSION

The integrated approach of different solver technologies allows to predicting a broad range of SCAL parameters under physical compression in a reasonable amount of time and memory. Our results point out that small compressions lead to very different material properties. That behavior should be considered for macroscopic simulations.

REFERENCES

1. H. Andrä, N. Combaret, J. Dvorkin, E. Glatt, H. Junehee, M. Kabel, Y. Keehm, F. Krzikalla, M. Lee, C. Madonna, M. Marsh, T. Mukerji, E. Saenger, R. Sain, N. Saxena, S. Ricker, A. Wiegmann and X. Zhan, „Digital rock physics benchmarks Part I: Imaging and segmentation," *Computers & Geosciences*, 2013 (43), pp. 25-32.
2. H. Andrä, N. Combaret, J. Dvorkin, E. Glatt, H. Junehee, M. Kabel, Y. Keehm, F. Krzikalla, M. Lee, C. Madonna, M. Marsh, T. Mukerji, E. Saenger, R. Sain, N. Saxena, S. Ricker, A. Wiegmann and X. Zhan, „Digital rock physics benchmarks Part II: Computing effective properties," *Computers & Geosciences*, 2013 (43), pp. 33-43.
3. L. Cheng, A. Wiegmann and S. Rief, „SIMPLE-FFT for flow computations in low porous micro-CT images," to be published.
4. A. Wiegmann and K. P. Bube, „The Explicit-Jump immersed interface method: Finite difference methods for PDE with piecewise smooth solutions," *SIAM Journal on Numerical Analysis*, 1997 (37), pp. 827-862.
5. A. Wiegmann and A. Zemitis, „EJ-Heat: A fast Explicit-Jump harmonic averaging solver for the effective heat conductivity of composite materials," Report of Fraunhofer ITWM, 2006.
6. V. P. Schulz, P. P. Mukherjee, J. Becker, A. Wiegmann and C. Wang, „Modeling of two-phase behavior in the gas diffusion medium of polymer electrolyte fuel cells via full morphology approach," *Journal of the Electrochemical Society*, 2007 (154), 4, pp. 419-426.
7. M. Hilpert and C. T. Miller, „Pore-morphology-based simulation of drainage in totally wetting porous media," *Advances in Water Resources*, 2001 (24), pp. 243-255.
8. J. Becker, V. Schulz and A. Wiegmann, „Numerical determination of two-phase material parameters of a gas diffusion layer using tomography images," *Journal of Fuel Cell Science and Technology*, 2008 (5), 2, pp. 21006-21014.
9. M. Kabel and H. Andrä, „Fast numerical computation of precise bounds of effective," Report of Fraunhofer ITWM, 2013 (224).
10. S. Linden, A. Wiegmann and H. Hagen, „The LIR space partitioning system applied to the Stokes equations," *Computer Aided Geometric Design*, submitted.